

# Revisiting Filtering of Two-line Element Sets for Higher Precision Ephemerides

Max I. Hallgarten La Casta<sup>(1)</sup>, Davide Amato<sup>(1)</sup>

<sup>(1)</sup>*Department of Aeronautics, Imperial College London  
London, United Kingdom*

*Emails: m.hallgarten-la-casta21@imperial.ac.uk, d.amato@imperial.ac.uk*

**Abstract** – The availability of accurate and timely state predictions for objects in near-Earth orbits is becoming increasingly important due to the growing congestion in key orbital regimes. The Two-line Element Set (TLE) catalogue remains, to this day, one of the few publicly-available, comprehensive sources of near-Earth object ephemerides. At the same time, TLEs are limited by their corresponding low-fidelity physical models, introducing errors and uncertainty into state predictions. Previous literature has shown that filtering TLEs with batch least squares methods can yield significant improvements in long-term state prediction accuracy. However, this process can be highly sensitive to TLE quality which can vary throughout the year. It will be shown that removing systematic biases in along-track position prior to state estimation can reduce post-fit position errors by an order of magnitude for selected satellites in the Medium Earth Orbit (MEO) regime.

## I. INTRODUCTION

The rise of the “New Space” era, driven by the growth in the number of commercial actors in the space domain, has led to a significant increase in the near-Earth Resident Space Object (RSO) population over the past decade, including year-on-year growth in the number of launches and payloads [1].

The growth in the RSO population has been seen primarily in the Low Earth Orbit (LEO) and Geostationary Earth Orbit (GEO) regimes, therefore the majority of these objects are concentrated into the same limited regions. The risk of collisions between RSOs continues to grow, highlighting the importance of improving the capacity and capabilities of Conjunction Assessment (CA) systems. These systems are highly dependent on accurate and precise state estimates to remain effective. With future exploration and development, the cislunar environment will become increasingly relevant, underscoring the need to understand various different orbital regimes.

Many operators have high precision state estimates for their own spacecraft based on their own on-board sensors, however they remain dependent on governmental and commercial Space Situational Awareness (SSA) organisations, and data sharing with other operators for state estimates of other objects. The financial cost of these services mean that smaller operators and academia remain reliant on publicly available sources, primarily the TLEs published by the United States Space Force (USSF).

One of the greatest advantages of TLEs is that they are freely available for a significant proportion of RSOs currently (and formerly) in near-Earth orbit. They represent an unparalleled source of data for RSO state vectors. Nevertheless, they are subject to a number of limitations which are difficult to overcome, primarily their limited accuracy when predicting states. This is due to the analytical models used by the format (SGP4 and SDP4) which use simplified perturbation models with limited fidelity [2]. This is despite the fact that TLEs themselves are generated by fitting the models to higher-order predictions made by direct Orbit Determination (OD) [3]. Additionally, the lack of uncertainty information for TLEs mean that their accuracy, even at epoch, remains effectively unknown. The result is a widely used data format with high availability across the orbital catalogue but with poor accuracy, making them unsuitable for precision applications.

Previous literature has demonstrated that it is possible to use TLEs in conjunction with higher fidelity orbital propagators to produce more accurate state estimations through Pseudo-Orbit Determination (P-OD). This is the process of conducting OD on products which themselves are the result of an OD process. Levit and Marshall [4] conducted batch least squares fitting of a high-fidelity numerical model to TLE pseudo-observations, improving state prediction accuracy in LEO from approximately 100 to 3000 m/day to 50 to 200 m/day. Vallado, Bastida Virgili, and Flohrer [5] extended existing analyses by investigating the influence of different estimation parameters, concluding that uncertainty was largest in the along-track direction and that force model fidelity had a limited impact on results. Bennett, Sang, Smith, and Zhang [6] demonstrated that relatively simple bias models can be used to improve TLE-based P-OD when fused with Satellite Laser Ranging (SLR) data. Chen and Lin [7] showed that fit prediction accuracy can be improved by restricting sampling to within two orbital periods of each epoch.

The limited fidelity of the SGP4 and SDP4 models was identified as an issue as TLEs became more widely used, particularly when considering “the requirements and problems in modern space mission operations” [8]. This led to the development of the SGP4-XP model, a new algorithm for propagating TLEs with greater precision, albeit with a reduction in computational performance [8]. An extension of SGP4 and SDP4, this updated model includes improved geopotential and resonance modelling, higher order lunisolar per-

turbations, a more detailed atmospheric model, and improved Solar Radiation Pressure (SRP) modelling [8]–[10]. It should be noted that TLEs using SGP4-XP, designated as Type 4 ephemerides, are not compatible with the original SGP4/SDP4 model, nor vice versa [8]. This is a product of the models being based on different averaging theories and, hence, they correspond to different dynamical systems.

Binaries for SGP4-XP are available from USSF; however, they do not publish compatible TLEs publicly. Nevertheless, testing with synthetically generated Type 4 TLEs has demonstrated significant improvements in prediction accuracy for objects in the MEO and GEO regimes [8]. One feature, particularly critical for P-OD, is the “more realistic dynamics coming from the SGP4-XP algorithm [yielding] a structure in the error which is more Gaussian than that of the classical SGP4” [8]. This includes a significant reduction in along-track error [9] which is the primary component of classical TLE error. Since Type 4 TLEs remain unavailable publicly, methods for reducing TLE biases remain an important area of investigation for deriving higher precision ephemerides.

## II. METHODOLOGY

### A. TLE Sampling

Object states are represented in TLEs as a set of mean elements (plus a ballistic coefficient) which correspond to a specific averaging theory, in this case a development of a theory originally developed by Kozai [2]. The osculating Cartesian state vector for a given object at a given time can be calculated with simplified general perturbation models used for the TLE format: SGP4 or SDP4. The latter is used for orbits with a period greater than 225 minutes, introducing deep space perturbations [11].

Occasionally, TLEs are re-issued for a given epoch but with updated orbital elements. This results in TLE data sets occasionally containing multiple TLEs at given epochs. In these cases, it is assumed that the most recently issued TLE is the most accurate, therefore a pre-filter is applied to drop any older duplicate TLEs.

A globally-spaced sampling strategy, as used by Levit and Marshall [4], was used to generate pseudo-observations from each set of TLEs, as illustrated in Fig. 1. The set of TLEs is sampled at equally spaced intervals throughout the fit window. For a sample point, the most recent TLE preceding it is used for generating

a pseudo-observation, switching over to the following TLE when passing its respective epoch. The first TLE is backpropagated for the sample points which lie between its epoch and the start of the fit window.

### B. TLE Smoothing

Sharp discontinuities in object state can be introduced when transitioning between TLEs due to the updated orbital elements. Nevertheless, for many objects in MEO and GEO, the dynamical model is sufficiently accurate that the size of these discontinuities is relatively small. Under the current implementation, no smoothing between TLEs is conducted as it is not expected to have a significant impact on fit quality.

Vallado, Bastida Virgili, and Flohrer noted that “TLEs possess potentially wide variability” [5] in quality. For a fit on a single poor quality TLE, this can have a significant impact on the performance of a fit with respect to the truth. However, the influence of a single “bad” TLE can be somewhat mitigated through the inclusion of multiple TLEs in the fit window [5].

### C. Test Satellites

Four test satellites were considered for initial testing: both pairs each of the Laser Geodynamics Satellite (LAGEOS) and Etalon satellites, as listed in Table 1. These test satellites were designed for geodesy and are covered in retro-reflectors which are designed to reflect beams of light back to their point of origin [12]. These allow ground-based laser systems to make highly precise ranging measurements (typically at the centimetre level) based on the two-way time-of-flight of laser pulses.

These test satellites were selected due to a number of advantages: their altitudes (in MEO) which reduced the influence of certain perturbations, such as atmospheric drag which is effectively not present; their high mass-to-area ratios which limited the effect of SRP; and, most importantly, their role as geodesy satellites which meant that accurate ephemerides were readily available for validating fit accuracy.

“Ground truth” data for the test satellites was provided by the International Lasing Ranging Service (ILRS). Post-processed, high-precision ephemerides derived from SLR is published via multiple channels, including NASA’s Crustal Dynamics Data Information System (CDDIS) and ESA’s Navigation Office.

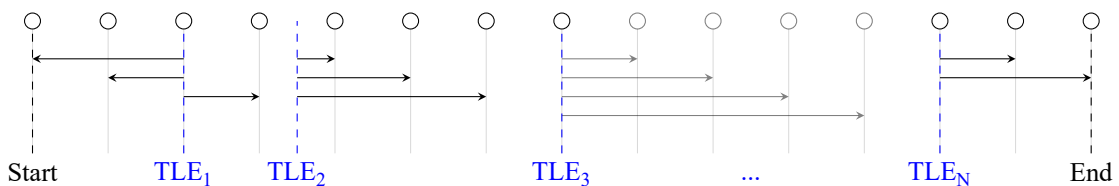


Fig. 1. TLE sampling strategy.

Table 1. Test satellites considered for P-OD.

Name	NORAD ID	SP3 ID	Semi-major axis [km]	Eccentricity [-]	Inclination [deg]
LAGEOS-1	8820	L51	12270	0.005	110
LAGEOS-2	22195	L52	12160	0.014	52.6
Etalon 1	19751	L53	25500	0.002	64.3
Etalon 2	20026	L54	25500	0.002	65.6

#### D. Physical Model

Computational performance was an important consideration as it is planned to extend this estimation process to the entire TLE catalogue. It was decided to use a “minimal model” where model parameters were tuned to minimise complexity and computational cost without significantly impacting the estimation process accuracy.

During initial testing, gravitational perturbations were found to be the most critical, therefore a geopotential model to account for the non-sphericity of the Earth, and third body perturbations resulting from the Moon and the Sun were included in the physical model. Several of the perturbations used by Levit and Marshall [4] were discarded, as listed in Table 2, as these have minimal impact in the MEO regime.

Numerical testing was conducted to determine the level of model fidelity required for effective P-OD of the test satellites without incurring significant computational cost. A convergence study was used to evaluate the influence of geopotential degree and order on propagations, using a high degree and order model (50-by-50) as a reference. It was found that a truncated 10-by-10 model was sufficient to achieve less than 10 m position error after 30 days of propagation with respect to the 50-by-50 geopotential model, which is adequate for this analysis. Similarly, solid tides were found to have a minimal effect on the satellites’ orbits. The test satellites’ altitudes meant that the influence of atmospheric drag was vanishingly small therefore a drag model was not included. The influence of SRP was evaluated by comparing propagations with various reflection coefficients, in the range of 0 to 3, against a propagation without SRP. It was found that the position error after 30 days did not exceed 20 m, even for the most perturbed case, confirming that the influence of SRP could be ignored for the test satellites.

Table 2. Comparison of perturbations with Levit and Marshall [4].

Perturbation	Levit and Marshall	Author
Geopotential	✓	✓
Solid tides	✓	
Third-bodies	✓	✓
Atmospheric drag	✓	
SRP	✓	

#### E. Trajectory Propagation

Cowell’s method was used to represent the perturbed motion of the satellites:

$$\ddot{\mathbf{r}} = -\frac{\mu}{\|\mathbf{r}\|^3}\mathbf{r} + \mathbf{F}(\mathbf{r}, \dot{\mathbf{r}}, t), \quad (1)$$

where  $\mathbf{r}$  is the position vector;  $\mu$  is the gravitational parameter of the central body; and  $\mathbf{F}(\mathbf{r}, \dot{\mathbf{r}}, t)$  is a vector function representing the non-Keplerian perturbing terms as a function of position ( $\mathbf{r}$ ), velocity ( $\dot{\mathbf{r}}$ ), and time ( $t$ ).

Propagation, and later state estimation as discussed below, was performed through the Orekit spaceflight library [13]. A 10-by-10 truncation of the EIGEN-6S gravity field model [14] was used for geopotential modelling. JPL’s DE441 planetary and lunar ephemerides [15] were used to generate state vectors for the Sun and Moon when calculating lunisolar perturbations.

Numerical integration was provided by a Dormand-Prince 8(5,3) integrator. This is a Runge-Kutta integrator with built-in error estimation and step size control, and continuous output [16]. For initial testing, the integrator was initialised with minimum and maximum step sizes of 0.1 s and 300 s, respectively, and a position error tolerance of 1 mm.

#### F. Batch Least Squares

The batch least squares estimator considers the problem of fitting a mathematical model to a set of observations. In this case, the mathematical model is the numerical model propagated to each observation time. The following derivation summarises the method as described by Vallado [17], and Tapley, Schutz, and Born [18].

The errors between the mathematical model and the observations is expressed as a set of residuals:

$$\mathbf{b} = \mathbf{y} - \mathbf{y}^*, \quad (2)$$

$$= \mathbf{y} - \mathbf{A}\mathbf{x}, \quad (3)$$

where  $\mathbf{b}$  is the residual vector;  $\mathbf{y}$  is the vector of (pseudo-)observations;  $\mathbf{y}^*$  is a vector of predictions;  $\mathbf{A} = \partial\mathbf{y}^*/\partial\mathbf{x}$  is the partial derivatives matrix of the system, in this case computed with finite differences as described by Vallado [17]; and  $\mathbf{x}$  is the decision vector, in this case the initial Cartesian state:

$$\mathbf{x} = \begin{bmatrix} \mathbf{r}_0 \\ \mathbf{v}_0 \end{bmatrix}, \quad (4)$$

where  $\mathbf{r}_0$  and  $\mathbf{v}_0$  are the initial position and state vectors, respectively. In this case, the first pseudo-observation is used to initialise the estimator as it is expected to be close to the optimal solution. Since atmospheric drag and SRP were not modelled, their corresponding parameters were not included as part of the estimation process.

The estimation process is expressed as an optimisation problem with the objective of minimising the sum of the square of the residuals:

$$\min_{\mathbf{x}} J(\mathbf{x}) = \frac{1}{2} \mathbf{b}^T \mathbf{W} \mathbf{b}, \quad (5)$$

$$= \frac{1}{2} (\mathbf{y} - \mathbf{A}\mathbf{x})^T \mathbf{W} (\mathbf{y} - \mathbf{A}\mathbf{x}), \quad (6)$$

where  $J(\mathbf{x})$  is the objective function, and  $\mathbf{W}$  is the weighting matrix, a diagonal matrix containing weights to account for the expected observation noise:

$$\mathbf{W} = \begin{bmatrix} \frac{1}{\sigma_1} & & & \\ & \frac{1}{\sigma_2} & & \\ & & \ddots & \\ & & & \frac{1}{\sigma_n} \end{bmatrix}, \quad (7)$$

where  $\sigma_i$  is the standard deviation of the measurement noise for the  $i$ -th observation variable.

It can be shown that the minimisation problem can be expressed as the solution to a linear system [17], [18]:

$$\hat{\mathbf{x}} = (\mathbf{A}^T \mathbf{W} \mathbf{A})^{-1} \mathbf{A}^T \mathbf{W} \mathbf{y}, \quad (8)$$

where  $\hat{\mathbf{x}}$  is the best estimate of the optimal decision vector. Due to the non-linearity of the dynamical system, the minimisation is iterated by re-linearising at each solution. This iteration continues until convergence is reached, in this case determined by the absolute difference between solutions reaching a set threshold.

The estimated covariance can be calculated based on the partial derivatives and weighting matrices:

$$\mathbf{P} = (\mathbf{A}^T \mathbf{W} \mathbf{A})^{-1}, \quad (9)$$

where  $\mathbf{P}$  is the fit covariance matrix. The sample covariance of the residual scatter can be used as an additional metric for fit uncertainty.

The weighting matrix was defined using TLE noise estimates from literature, as presented in Table 3 in the Radial, Transverse, Normal (RTN) frame. The weights are defined by standard deviations in inertial space, therefore for each epoch, the uncertainties were rotated from the RTN frame to the inertial frame of the corresponding pseudo-observation. The cross-correlation components were ignored.

### G. Fit Quality Evaluation

The primary metric used for evaluating fit quality and prediction accuracy was post-fit position Root-mean-

Table 3. Mean TLE uncertainty in the RTN frame at epoch, for “enhanced” TLEs released after 2013. Adapted from [19].

Type	$\sigma_R$	$\sigma_T$	$\sigma_N$
Position [m]	$1.2 \times 10^2$	$2.0 \times 10^3$	$8.0 \times 10^1$
Velocity [m/s]	$2.4 \times 10^0$	$1.3 \times 10^{-1}$	$6.8 \times 10^{-2}$

square Error (RMSE):

$$\Delta r_{\text{RMSE}} = \sqrt{\frac{1}{N} \sum_i^N \|\mathbf{r}_i^* - \mathbf{r}_i\|^2}, \quad (10)$$

where  $N$  is the number of samples; and  $\mathbf{r}_i^*$  and  $\mathbf{r}_i$  are the predicted and true states, respectively, at the  $i$ -th epoch.

Covariances resulting from the estimation process were compared by considering the size of the region of uncertainty. The volume of the multivariate Gaussian uncertainty distribution is that of an ellipsoid:

$$V_{1\sigma} = \frac{4}{3} \pi (\sigma_{r,1}) (\sigma_{r,2}) (\sigma_{r,3}), \quad (11)$$

where  $V_{1\sigma}$  is the volume of the 1- $\sigma$  position covariance matrix; and  $\sigma_{r,1}$ ,  $\sigma_{r,2}$ , and  $\sigma_{r,3}$  are the position standard deviations in the principal axes, i.e., the eigenvalues of the position covariance matrix.

As an uncertainty metric, we consider the equivalent radius of the uncertainty ellipsoid, that is the radius of a sphere with the same volume as the 1- $\sigma$  ellipsoid:

$$R_{1\sigma} = \sqrt[3]{(\sigma_{r,1}) (\sigma_{r,2}) (\sigma_{r,3})}. \quad (12)$$

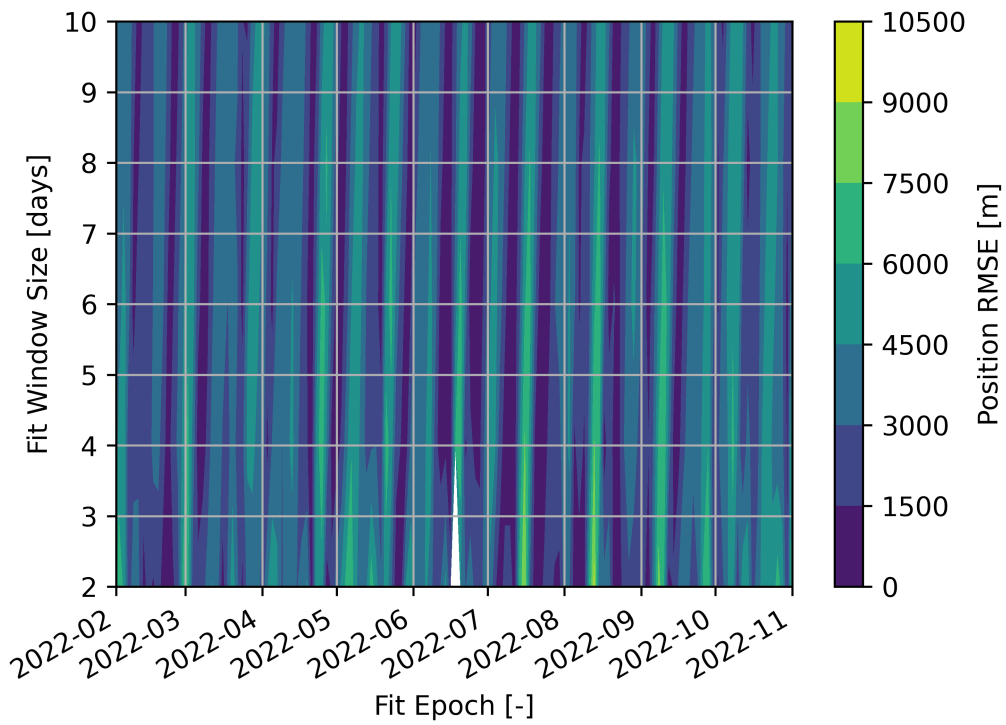
## III. RESULTS

### A. Parameter Sensitivity

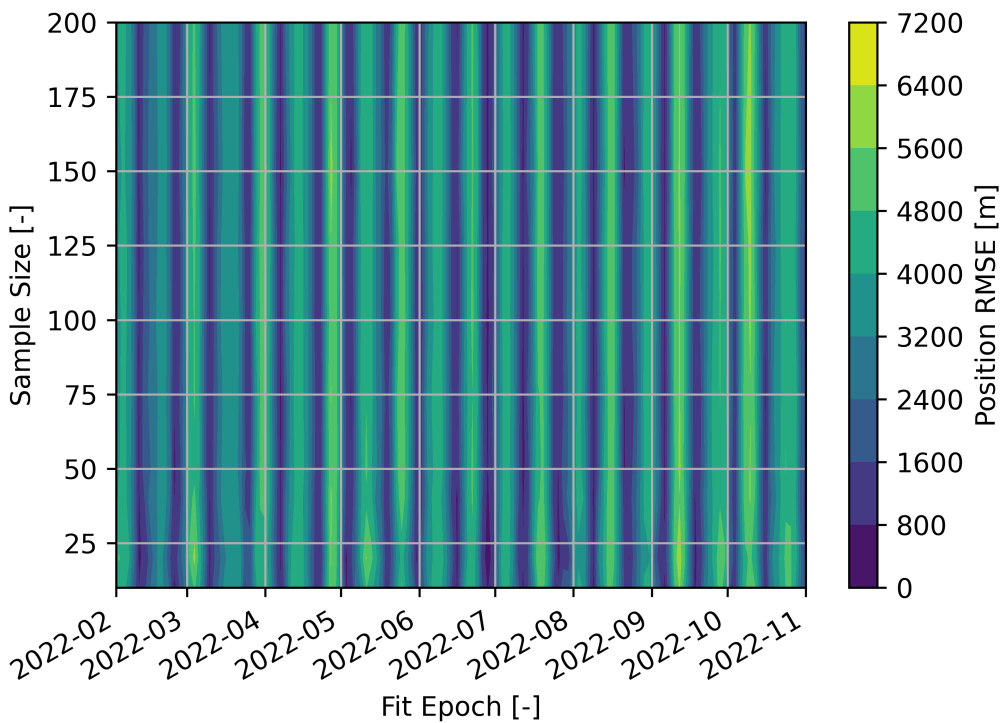
A parameter sensitivity study was conducted to investigate the influence of fit parameters on fit accuracy. Three parameters were considered: the fit epoch, the size of the fit window, and the the number of samples in the window. Permutations of fit epoch and fit window size with a fixed number of samples, and fit epoch and sample size with a fixed fit window size were evaluated by conducting fits, followed by a propagation for 30 days post-fit.

The results of the parameter sensitivity study for Etalon 1, throughout the year 2022, are presented in Fig. 2. These plots illustrate the position RMSE achieved by a fit at a given epoch (defined as the end of the window), as a function of fit window size and sample size in Figs. 2a and 2b, respectively. Similar results were observed for all four of the test satellites.

The size of the window had a limited impact on the fit accuracy, as illustrated by the limited variation in position RMSE at a given fit epoch. Varying the number of



(a) Varying fit window size for a fixed 100 sample points.



(b) Varying sample size for a fixed 10 day fit window.

Fig. 2. Position RMSE during the 30 days post-fit for Etalon 1.

samples showed similar behaviour as the parameter had limited influence on the position RMSE. The fit epoch, however, appeared to be a significant driver for fit quality, visible at periodic banding of low and high position RMSEs throughout the year. This banding results from the presence of systematic biases within the TLEs affecting the results of the fit process and, subsequently, post-fit prediction accuracy.

### B. TLE debiasing

Systematic biases in the TLEs were suspected to cause significant variation in fit quality throughout the year. Ly, Lucken, and Giolito [20] highlighted seasonal and periodic variations in TLE quality, primarily affecting the along-track component of the satellite's position.

To demonstrate the concept of TLE debiasing, a simplified sinusoidal model was proposed for estimating along-track error:

$$\Delta\theta_T(t) \approx a \sin\left[\frac{2\pi}{b}(t+c)\right] + d, \quad (13)$$

where  $\Delta\theta_T = \Delta r_T/r$  is the transverse angular error;  $a$ ,  $b$ ,  $c$ ,  $d$  are the model amplitude, period, phase offset, and mean offset, respectively; and  $t$  is the time, in this case defined as an offset from a given epoch.

The fitted parameters for each of the test satellites are presented in Table 4 and the corresponding models illustrated in Fig. 3. The Etalon 1 and 2 satellites showed good agreement with the model, with their respective parameters; however, LAGEOS-1 showed slightly different behaviour with an additional longer term variation, while LAGEOS-2 showed a complete lack of agreement with the simplified model.

### C. Prediction Accuracy

The 30 day post-fit position RMSEs for 10 day, 100 sample fits are presented in Fig. 4. This includes results both with and without TLE debiasing.

The four satellites demonstrated differing levels of fit performance. LAGEOS-1 had the lowest position RMSEs, remaining below  $10^3$  m throughout the year. Etalon 1 and 2 had RMSEs typically higher than the LAGEOS satellites, remaining between  $6 \times 10^2$  to  $8 \times 10^3$  m throughout the year. The respective RMSEs of LAGEOS-1, Etalon 1, and Etalon 2 had similar behaviour, oscillating about a mean throughout the year with

a repeat period of approximately two weeks. LAGEOS-2, on the other hand, showed a decreasing RMSE during the latter half of the year, with peak RMSE reducing from approximately  $4 \times 10^3$  m to  $10^3$  m.

TLE debiasing had a significant impact on position RMSEs for LAGEOS-1, Etalon 1, and Etalon 2 with typical reductions by approximately an order of magnitude. The debiasing process also affected the smoothness of the variation throughout the year. Sharper changes in RMSE were visible, although some periodic features were retained. The LAGEOS-2 fits remained largely unaffected by the debiasing process, however this was expected due to the small amplitude of its error model.

### D. Residual Covariance

The equivalent radii of the residual covariances resulting from fits of the LAGEOS and Etalon satellites are presented in Fig. 5.

LAGEOS-1 had the smallest and most consistent equivalent radius, constant at 50 m other than for a small increase during July. Etalon 1 and 2 had periodic variations throughout the year in a band from 100 to 200 m. The oscillations in uncertainty were correlated with each other, showing similar frequency and phase. The equivalent radius for LAGEOS-2 reduced in the latter half of the year from a 100 to 150 m band to below 100 m.

TLE debiasing appeared to have little effect on the residual covariances of any of the test satellites. There were no significant changes in magnitudes nor structure with only small variations, in the order of metres, for some fits of Etalon 1 and 2.

## IV. DISCUSSION

The period of the along-track error model had significant agreement between LAGEOS-1, and Etalon 1 and 2 at approximately 27.5 days. This is very close to the Moon's orbital period (approximately 27.3 days), supporting the suggestion that mismodelling of the Moon's third-body perturbation is a contributing factor to the along-track error, as identified by Ly, Lucken, and Giolito [20]. The mismodelling error may result from either, or a combination of, the lunar ephemerides used by SDP4 or a lack of lunar short-periodic terms. Preliminary testing suggested that the envelope of lunar short-periodic terms show similar magnitude to that of the observed biases. The phase offsets also showed good

Table 4. Fitted parameters for the bias model, expressing time in days since midnight on the 1<sup>st</sup> January 2022.

Satellite	$a$ [rad]	$b$ [days]	$c$ [days]	$d$ [rad]
LAGEOS-1	$1.41 \times 10^{-5}$	27.5	$6.82 \times 10^{-2}$	$-1.79 \times 10^{-8}$
LAGEOS-2	$2.28 \times 10^{-6}$	26.6	$-1.19 \times 10^1$	$-4.00 \times 10^{-6}$
Etalon 1	$4.82 \times 10^{-5}$	27.5	$-9.17 \times 10^{-1}$	$-4.43 \times 10^{-7}$
Etalon 2	$6.75 \times 10^{-5}$	27.6	$-1.80 \times 10^{-1}$	$7.79 \times 10^{-8}$

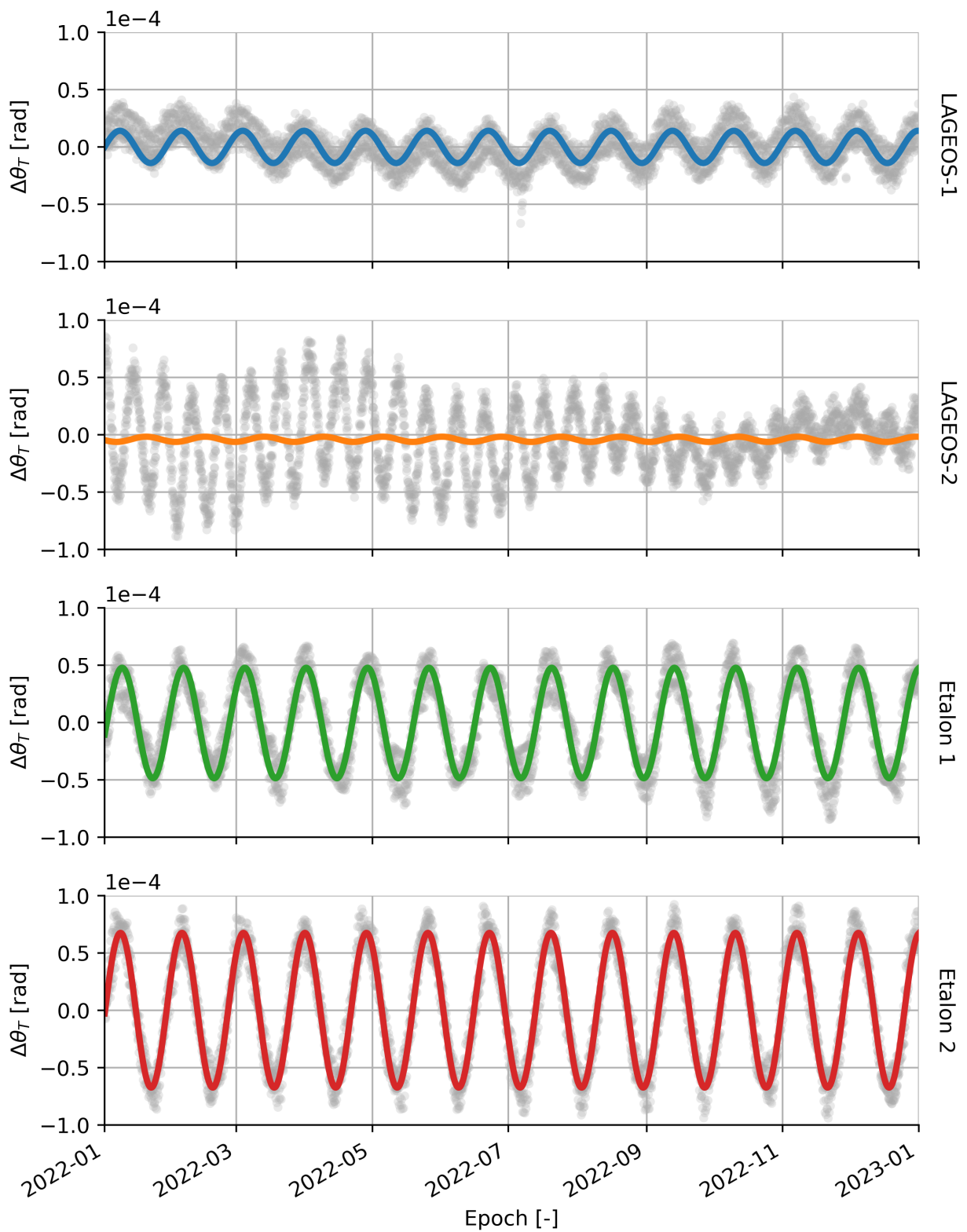


Fig. 3. Transverse angular errors of TLEs with respect to SLR, with the data points and fitted models in grey and colour, respectively.

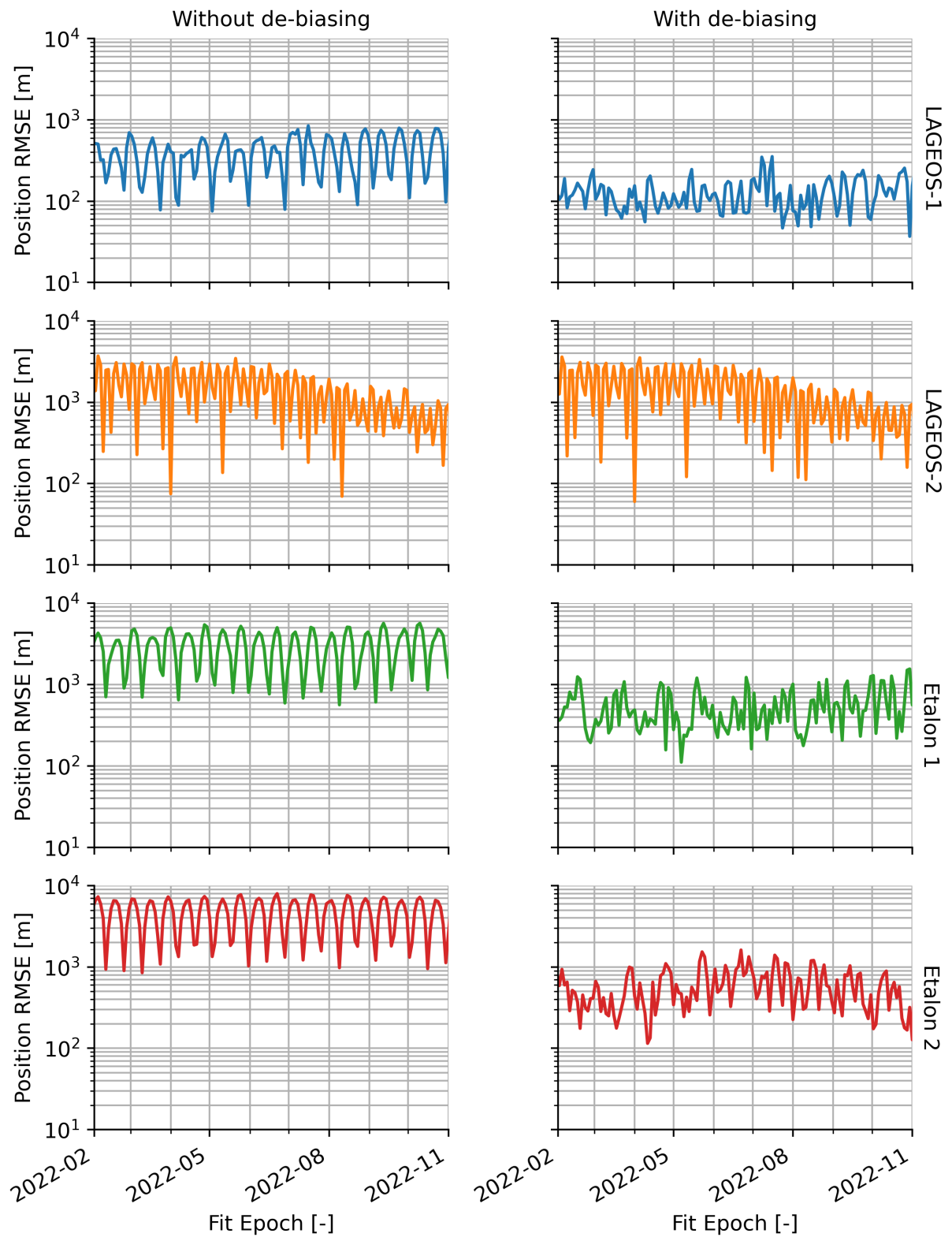


Fig. 4. Position RMSE post-fit for the LAGEOS and Etalon satellites as a function of fit epoch. Each fit window contained 100 sample points over a 10 day period.

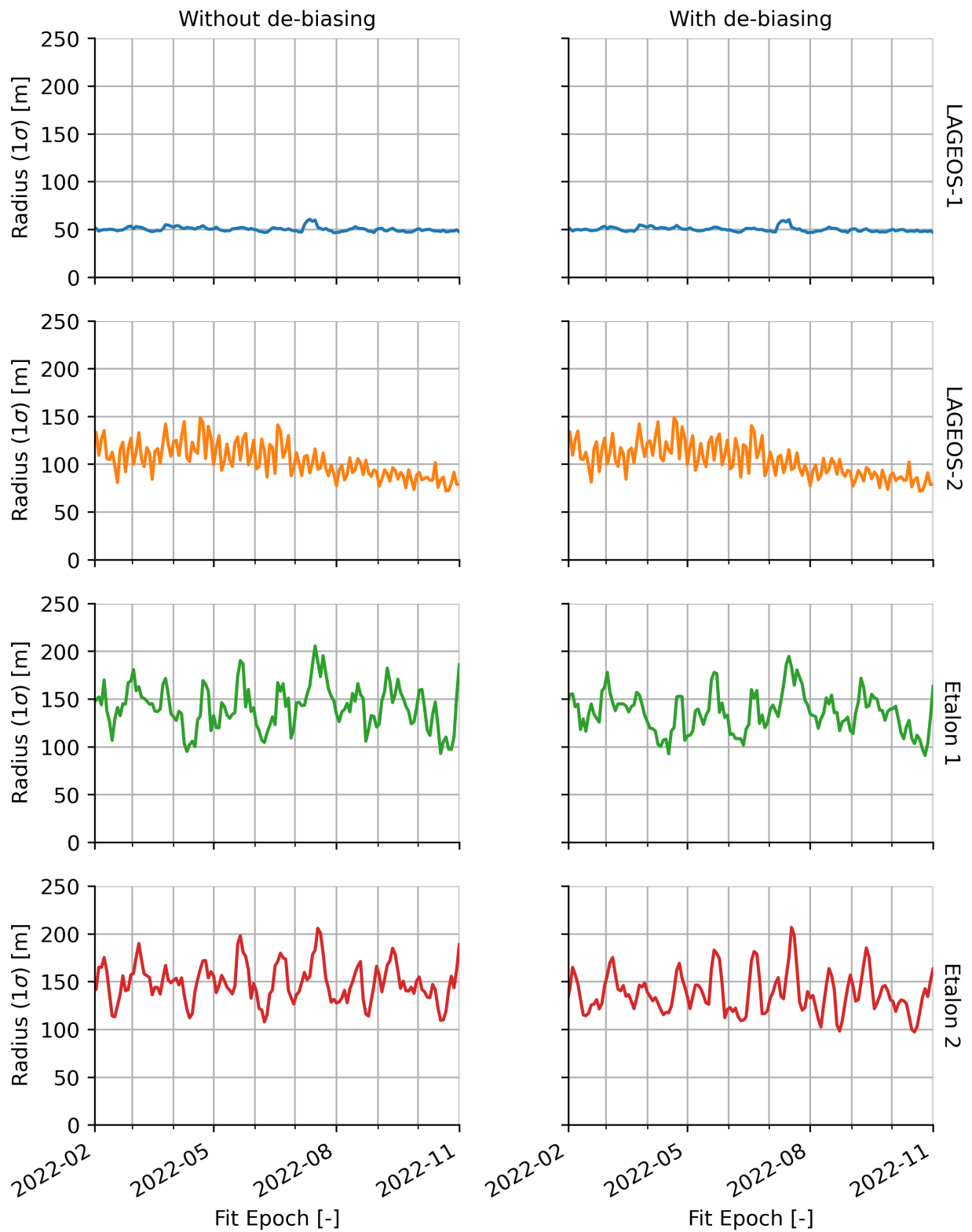


Fig. 5. Equivalent radius of the position residuals covariance matrix for the LAGEOS and Etalon satellites, calculated via the volume-equivalent sphere. Each fit window contained 100 samples points over a 10 day period.

agreement, varying by less than one day between the satellites, suggesting that it may be possible to constrain these parameters to constants across all of the satellites.

The main limitation of the along-track error model was that it was not generalised for any satellite: model amplitudes varied by satellite, and LAGEOS-1 showed slightly different behaviour to the Etalon satellites. The outlying behaviour of LAGEOS-2 raises the question of whether other satellites will have similar behaviour, and whether it is a direct result of the SDP4 model, the dynamics of specific orbital regimes, or additional non-physical factors introduced during the TLE generation process. Additional components of the state vector may benefit also from debiasing: although not implemented here, the radial velocity was found to have similar periodic variations with respect to epoch.

The systematic variation in along-track error means that the biases in successive TLEs are highly correlated. The period of this variation is much longer than the typical sizes of the fit windows, therefore the pseudo-observations will have similar, correlated biases. In effect, the biased TLEs are representing physically accurate and consistent orbits, however not matching the true orbits of the satellites. The debiasing process reduces the mean error of the pseudo-observations with respect to the true state, however the noise remains unaffected. This highlights that the covariance cannot be used as an indicator for fit accuracy as it is unaffected by the biases.

Data-driven solutions, such as the simplified model presented here or other machine learning methods [20], are limited to the availability of “ground truth” data, such as from SLR or post-processed pseudorange, for training, validation, and testing. It is highly probable that these models cannot be extrapolated to other satellites nor are there accurate methods for testing this. Furthermore, it is unknown whether these higher accuracy products are used during the TLE generation process and whether this means that these satellites have TLE sets with differing characteristics.

## V. FUTURE WORK

Although the simple sinusoidal model was effective at debiasing TLE both Etalon 1 and 2, it required different model parameters for each satellite and analysis including an SLR-based “ground truth”. Future implementations will need to focus on providing a more generalised solution, preferably without requiring SLR data to enable its extension to the rest of the TLE catalogue.

The current analysis was limited to only four satellites in MEO and may not represent general TLE behaviour at these altitudes. There are additional test satellites available in this orbital regime with precision ephemerides which could be used for further investigation, namely Global Navigation Satellite System (GNSS) satellites. These have similar orbits to the Etalon satellites, in terms

of semi-major axis, eccentricity, and inclination. Nevertheless, these satellites are active and able to manoeuvre, which will need to be taken into account by any analysis of their TLEs.

It is expected that TLE behaviour will be different in LEO due to the changes in perturbations model, notably the removal of lunisolar perturbations and SRP, but the inclusion of atmospheric drag. A separate investigation into the biases present in this orbital regime will be required. It is expected that the same systematic biases seen with MEO test satellites will not be present, instead replaced by issues with drag estimation.

Several of the limitations of batch least squares methods can be addressed by sequential filters; therefore, these are the logical next step for improving TLE-based P-OD. These types of filters lend themselves naturally to solution updates as new TLEs are published by USSF, and allow for physical parameters to be included in the estimation process continuously, such as ballistic coefficient for LEO. It is proposed to use an Unscented Kalman Filter (UKF), initialised with an initial state and covariance from a batch least squares solution. Nevertheless, it should be noted that both batch least squares methods and sequential filters will be susceptible to biases in the pseudo-observations without the ability to detect degraded estimates through the covariance. TLE biases must be addressed before conducting any P-OD.

## VI. CONCLUSIONS

Systematic along-track biases throughout the year were identified as the primary limiting factor in the quality of P-OD fits in the MEO regime. Mitigation of these biases was demonstrated to be key for improving the quality of higher precision ephemerides derived from TLEs. A simple sinusoidal model for estimating along-track error was effective at reducing the typical post-fit accuracy by an order of magnitude for selected test satellites.

It has been shown that the covariance output from the P-OD process cannot be used to evaluate the prediction accuracy of a given fit. Uncorrected TLE-based pseudo-observations in the MEO regime do not follow a Gaussian distribution about the true state of a satellite, an assumption required for many state estimation algorithms. This results in fits which appear well correlated with pseudo-observations but, in reality, are poorly correlated with the true underlying state.

The TLE catalogue remains one of the few sources of ephemerides for a significant proportion of RSOs in near-Earth orbits. Until Type 4 TLEs are released publicly for a critical share of the catalogue, a combination of debiasing and P-OD will be required for deriving higher-precision ephemerides for many RSOs. The development of generalised bias estimation models, covering multiple orbital regimes, will be crucial for improving TLE-based P-OD.

## VII. REFERENCES

- [1] “ESA’s Annual Space Environment Report,” ESA Space Debris Office, Darmstadt, Germany, 12th Sep. 2023. [Online]. Available: [https://www.sdo.esoc.esa.int/environment\\_report/Space\\_Environment\\_Report\\_latest.pdf](https://www.sdo.esoc.esa.int/environment_report/Space_Environment_Report_latest.pdf) (visited on 07/02/2024).
- [2] F. R. Hoots, P. W. Schumacher and R. A. Glover, “History of Analytical Orbit Modeling in the US Space Surveillance System,” *Journal of Guidance, Control, and Dynamics*, vol. 27, no. 2, pp. 174–185, 2004.
- [3] M. D. Hejduk, S. J. Casali, D. A. Cappellucci, N. L. Ericson and D. E. Snow, “A catalogue-wide implementation of general perturbations orbit determination extrapolated from higher order orbital theory solutions,” presented at the AAS/AIAA Spaceflight Mechanics Meeting, Kauai, HI, USA, August 2013.
- [4] C. Levit and W. Marshall, “Improved orbit predictions using two-line elements,” *Advances in Space Research*, vol. 47, no. 7, pp. 1107–1115, 2011.
- [5] D. A. Vallado, B. Bastida Virgili and T. Flohrer, “Improved SSA through orbit determination of Two-Line-Element sets,” presented at the 6th European Conference on Space Debris, Darmstadt, Germany, April 2013.
- [6] J. C. Bennett, J. Sang, C. Smith and K. Zhang, “Improving low-Earth orbit predictions using two-line element data with bias correction,” presented at the Advanced Maui Optical and Space Surveillance Technologies Conference, Maui, HI, USA, Sep. 2012.
- [7] J. Chen and C. Lin, “Research on Enhanced Orbit Prediction Techniques Utilizing Multiple Sets of Two-Line Element,” *Aerospace*, vol. 10, no. 6, p. 532, 2023.
- [8] D. Conkey and M. Zielinski, “Assessing Performance Characteristics of the SGP4-XP Propagation Algorithm,” presented at the Advanced Maui Optical and Space Surveillance Technologies Conference, Maui, HI, USA, Sep. 2022.
- [9] T. Payne, F. Hoots, A. Butkus, Z. Slatton and D. Nguyen, “Improvements to the SGP4 propagator (SGP4-XP),” presented at the Advanced Maui Optical and Space Surveillance Technologies Conference, Maui, HI, USA, Sep. 2022.
- [10] A. Holincheck and J. Cathell, “Improved Orbital Predictions using Pseudo Observations - Maximizing the Utility of SGP4-XP,” presented at the Advanced Maui Optical and Space Surveillance Technologies Conference, Maui, HI, USA, Sep. 2021.
- [11] D. Vallado, P. Crawford, R. Hujsak and T. Kelso, “Revisiting Spacetrack Report #3,” presented at the AIAA/AAS Astrodynamics Specialist Conference and Exhibit, Keystone, CO, USA, August 2006.
- [12] M. Pearlman, D. Arnold, M. Davis, F. Barlier, R. Biancale, V. Vasiliev, I. Ciufolini, A. Paoletti, E. C. Pavlis, K. Sośnica and M. Bloßfeld, “Laser geodetic satellites: a high-accuracy scientific tool,” *Journal of Geodesy*, vol. 93, no. 11, pp. 2181–2194, 2019.
- [13] L. Maisonobe, V. Pommier and P. Parraud, “Orekit: an Open-source Library for Operational Flight Dynamics Applications,” presented at the 4th ICATT International Conference on Astrodynamics Tools and Techniques, Madrid, Spain, May 2010.
- [14] C. Förste, S. L. Bruinsma, R. Shako, O. Abrikosov, F. Flechtner, C. Dahle, H. Neumeyer, F. Barthelmes, R. Biancale, G. Balmino and R. König, “A new release of EIGEN-6: The latest combined global gravity field model including LAGEOS, GRACE and GOCE data from the collaboration of GFZ Potsdam and GRGS Toulouse,” in *Geophysical Research Abstracts*, vol. 14, 2012.
- [15] R. S. Park, W. M. Folkner, J. G. Williams and D. H. Boggs, “The JPL Planetary and Lunar Ephemerides DE440 and DE441,” *The Astronomical Journal*, vol. 161, no. 3, p. 105, 2021.
- [16] CS GROUP. “DormandPrince853Integrator (Hipparchus 3.0 API).” (2023), [Online]. Available: <https://www.hipparchus.org/apidocs/org/hipparchus/ode/nonstiff/DormandPrince853Integrator.html> (visited on 06/02/2024).
- [17] D. A. Vallado, *Fundamentals of Astrodynamics and Applications*, 4th ed. Hawthorne, CA, USA: Microcosm Press, 2013.
- [18] B. D. Tapley, B. E. Schutz and G. H. Born, *Statistical orbit determination*. Amsterdam, the Netherlands: Elsevier Academic Press, 2004.
- [19] J. Geul, E. Mooij and R. Noomen, “TLE uncertainty estimation using robust weighted differencing,” *Advances in Space Research*, vol. 59, no. 10, pp. 2522–2535, 2017.
- [20] D. Ly, R. Lucken and D. Giolito, “Correcting TLEs at epoch: Application to the GPS constellation,” *Journal of Space Safety Engineering*, Space Debris: The State of Art, vol. 7, no. 3, pp. 302–306, 2020.